Environmental Science and Pollution Research (2021) 28:18342–18353
https://doi.org/10.1007/s11356-020-09563-w

IMPACTS IN ENVIRONMENTAL TRENDS, HEALTH AND WELL BEING: A GLOBAL POLLUTION PROBLEM

Uranium and neptunium retention mechanisms in *Gallionella ferruginea*/ferrihydrite systems for remediation purposes

Evelyn Krawczyk-Bärsch[1] · Andreas C. Scheinost[1,2] · André Rossberg[1,2] · Katharina Müller[1] · Frank Bok[1] · Lotta Hallbeck[3] · Jana Lehrich[1] · Katja Schmeide[1]

Received: 13 January 2020 / Accepted: 1 June 2020
© ©The Author(s) 2020, corrected publication 2021

Abstract

The ubiquitous β-Proteobacterium *Gallionella ferruginea* is known as stalk-forming, microaerophilic iron(II) oxidizer, which rapidly produces iron oxyhydroxide precipitates. Uranium and neptunium sorption on the resulting intermixes of *G. ferruginea* cells, stalks, extracellular exudates, and precipitated iron oxyhydroxides (BIOS) was compared to sorption to abiotically formed iron oxides and oxyhydroxides. The results show a high sorption capacity of BIOS towards radionuclides at circumneutral pH values with an apparent bulk distribution coefficient (K_d) of 1.23×10^4 L kg^{-1} for uranium and 3.07×10^5 L kg^{-1} for neptunium. The spectroscopic approach by X-ray absorption spectroscopy (XAS) and ATR FT-IR spectroscopy, which was applied on BIOS samples, showed the formation of inner-sphere complexes. The structural data obtained at the uranium L_{III}-edge and the neptunium L_{III}-edge indicate the formation of bidentate edge-sharing surface complexes, which are known as the main sorption species on abiotic ferrihydrite. Since the rate of iron precipitation in *G. ferruginea*-dominated systems is 60 times faster than in abiotic systems, more ferrihydrite will be available for immobilization processes of heavy metals and radionuclides in contaminated environments and even in the far-field of high-level nuclear waste repositories.

Keywords Actinides · Sorption · Microorganism · Bacteriogenic iron oxyhydroxides · XAS · ATR FT-IR spectroscopy

Introduction

It is well known that in many freshwater and marine environments, where the oxygen concentrations can be very low (e.g., at anoxic-oxic transition zones), microaerophilic iron(II) oxidizers are common (Emerson and Moyer 1997; Edwards et al. 2003). Whereas abiotic iron oxidation is retarded at low oxygen concentrations, certain specialized species of iron oxidizers (e.g., *Gallionell*a spp.) are able to grow (Edwards et al. 2003), thus contributing to iron oxidation. Phylogenetically, these bacteria belong to the phylum Proteobacteria, which includes the freshwater genera *Leptothrix* (Fleming et al. 2011), *Gallionella* (Kucera and Wolfe 1957), and *Sideroxydans* (Weiss et al. 2007) as well as the marine genus *Mariprofundus* (Singer et al. 2011; Melton et al. 2014). Microbial iron(II) oxidation by microaerophilic iron(II) oxidizers at low oxygen concentrations occurs according to the following stoichiometric equation (Melton et al. 2014):

$$4Fe^{2+} + 10H_2O + O_2 \rightarrow 4Fe(OH)_3 + 8H^+ \quad (1)$$

The reaction is similar to the physico-chemical reaction in abiotic systems (Ankrah and Søgaard 2009). Decisive factors as to whether the precipitation of iron oxyhydroxide is going to be biotic or abiotic are redox potential and pH value. The iron(II)-oxidizing bacterium *Gallionella*, for example, requires a lower pH and a lower redox potential than commonly

The original online version of this article was revised due to a retrospective Open Access order.

Responsible editor: Georg Steinhauser

✉ Evelyn Krawczyk-Bärsch
E.Krawczyk-Baersch@hzdr.de

[1] Helmholtz-Zentrum Dresden-Rossendorf, Institute of Resource Ecology, Bautzner Landstr. 400, 01328 Dresden, Germany

[2] The Rossendorf Beamline, ESRF, F-38043 Grenoble, France

[3] Microbial Analytics Sweden AB (MICANS), SE-43535 Mölnlycke, Sweden

Published online: 16 June 2020

necessary for abiotic formation of iron oxyhydroxide (Hanert 1992; Søgaard et al. 2000). By thermodynamic analysis of the electrochemical equilibrium, the theoretical boundary between the field of ferrous solubility and the formation of biogenic ferric precipitates was defined by Ankrah and Søgaard (2009). Ferric iron precipitates rapidly due to the low solubility of ferric iron compounds in the area characterized by a pH range from 5.5–8.0 with a redox potential limit, moving from + 420 to + 50 mV. Eggerichs et al. (2014) defined the ferrous iron oxidation by *Gallionella*, which increases with increasing ferrous iron concentrations, showing a Michaelis-Menten-like distribution with $K_{Fe(II)} = 2.61 \pm 1.67$ mg L^{-1}, which is typical for iron-rich natural waters. In their studies about pH dependencies, the authors conclude that compared to abiotic oxidation, iron oxidation by *Gallionella* occurs within a much broader pH/oxygen range. There are different explanations for the bacteriogenically induced oxidation of ferrous iron. After Banfield et al. (2000), bacteria such as the *Gallionella* spp. and the *Leptothrix* spp. are able to oxidize enzymatically dissolved ferrous iron. Melton et al. (2014) assumed that the iron(II) oxidation may be carried out by an outer cell membrane iron(II)-oxidizing protein to prevent ferric iron mineral precipitation inside the cell. After Søgaard et al. (2000), the precipitation takes place in contact with the exopolymers, which act as catalysts for the oxidation-precipitation process of iron. This assumption is supported by the fact that biogenic ferric iron has a much higher density than physico-chemically precipitated colloidal ferrihydrite. Søgaard et al. (2000) assume that this phenomenon can be attributed to the fact that biogenically precipitated ferric iron is in contact with exopolymers. Soluble ferrous iron either adsorbs directly on the surface of exopolymers, where it becomes oxidized, or is attached to the exoploymers of *Gallionella ferruginea* in a colloidal form (Ankrah and Søgaard 2009). Thus, iron is oxidized and precipitates with a rate about 60 times faster than that in the abiotic process. The faster kinetic indicates a catalytic activity due to the presence of exopolymers from *G. ferruginea* (Søgaard et al. 2000), causing a rapid oxidation and formation of insoluble ferric hydroxides (Ankrah and Søgaard 2009). In a recent study, Hallbeck and Pedersen (2014) mentioned that whether the iron oxidation on the stalk is enzymatic or whether the stalk acts as a surface catalyst for the oxidation reaction is not known. Most of the 2- to 3-nm diameter-formed particles are attached to the surrounding negatively charged polymers (e.g., *Gallionella* stalks) or are flocculated to form colloidal aggregates (Banfield et al. 2000) and coatings on other mineral particles.

The minerals formed include two-line ferrihydrite, a nanoscale ferric iron oxyhydroxide mineral with the formula of $Fe_{10}O_{14}(OH)_2$ (Melton et al. 2014), lepidocrocite (Chan et al. 2011), and akageneite (Chan et al. 2004). These mineral phases are characterized by large surfaces, which are known to provide active adsorption sites for inorganic and organic contaminants. Iron oxyhydroxide minerals in general are found ubiquitously in the environment, where high concentrations of ferric iron are produced by either chemical oxidation or bacterial oxidation of ferrous iron (Ferris et al. 1989), e.g., in soils; weathered rocks; sediments; and water column of lakes, rivers, and oceans. Moreover, they are also present in contaminated soils and groundwater, resulting, e.g., from mining and milling activities, engineered nuclear waste environments, and nuclear decommissioning, where heavy metals and radionuclides were already released into the environment, thus posing a danger to humans and animals due to an ultimate potential incorporation into the food chain. Some authors (Pedersen and Karlsson 1995; Pedersen 1997; Ferris et al. 1999; Hallbeck and Pedersen 2005; Anderson et al. 2006) described biofilms formed in open fracture zones and on tunnel walls at the Äspö Hard Rock Laboratory (HRL) in the south-east of Sweden, where groundwater, including biological materials, is seeping in. The biofilms are predominantly formed by the indigenous iron-oxidizing bacterium *Gallionella* with up to 90 wt% precipitated ferric oxyhydroxide, thus providing an abundant surface area with remarkable highly reactive surface sites (Ferris et al. 1989; Nelson et al. 1995; Ferris et al. 2000; Anderson and Pedersen 2003). As a consequence, the biofilms can act as dominant sorbents for significant amounts of dissolved metals under certain environmental conditions, e.g., redox potential and pH (Ferris et al. 1989; Nelson et al. 1995). At near-neutral pH, the biogenically produced iron oxyhydroxides have the potential to adsorb 30–15,000 times more lanthanides than abiotic and synthetic iron oxyhydroxides (Anderson and Pedersen 2003). They may be more reactive sorbents also for contaminants, such as arsenic and chromium as recent studies showed. The sorption of arsenic(V) to biogenically produced iron oxyhydroxides was approximately three times higher than what was observed for synthetic 2-line ferrihydrite (Sowers et al. 2017). Whitaker et al. (2018) mentioned that biogenically produced iron oxyhydroxides may enhance chromium(VI) adsorption and even reduction. The authors attributed the higher adsorption property to the poorly ordered structures, large surface areas, and incorporation of cell-derived organic matter. The Äspö HRL is of particular interest for researchers, since the facility serves as an analog for a final nuclear waste repository for high-level radioactive waste. In the event of ingress of water, bacteriogenically produced iron oxyhydroxides may offer an additional barrier to the migration of dissolved radionuclides, which might be released from within the waste containers. Whereas a lot of previous investigations were performed to quantify metal ion sorption, there is still a lack concerning the identification of surface complexes and the determination of the structural coordination of sorption complexes on biogenically formed iron oxyhydroxides. The present study aims at responding to these points using spectroscopic methods for the molecular scale structural characterization, i.e., extended X-ray absorption fine structure (EXAFS) and in situ attenuated total reflection

Fourier-transform infrared (ATR FT-IR) spectroscopy. We focused our studies in the present work on two problematic α-emitting radionuclides, uranium and neptunium, which are characterized by long half-lives (^{238}U 4.47 × 10^9 years, ^{237}Np 2.14 × 10^6 years) and high radio- and chemotoxicity. Uranium occurs in the environment as a consequence of mining activities, leaching of radioactive wastes, and as a contaminant at nuclear legacy sites. Under aerobic conditions, uranium(VI) is mobile due to its high solubility. Under anaerobic conditions, uranium is typically reduced to poorly soluble uranium(IV). In geological disposal facilities, containing spent nuclear fuel, uranium will be the most significant radionuclide by mass (Marshall et al. 2014). In case of an accident, it might be released from within the waste containers. The oxidation state, speciation, and migration or immobilization behavior of uranium and radionuclides resulting from its radioactive decay will then depend on the surrounding conditions (e.g., pH, redox potential, oxygen concentration). Neptunium is one of the most important radionuclides of concern for long-term emplacement of nuclear waste due to its long half-life. The concentration of ^{237}neptunium will increase with time due to the radioactive decay of ^{241}plutonium and ^{241}americium (Kaszuba and Runde 1999; Lloyd et al. 2000). In oxic environments, aqueous neptunium speciation is dominated by the pentavalent cation, NpO_2^+ in the pH range 5 to 8 (Girvin et al. 1991) and at redox potentials between 100 and about 800 mV (Lieser and Mühlenweg 1988). Under anaerobic conditions neptunium(V) is reduced to the tetravalent form as sparingly soluble $Np(OH)_4$.

In the present study a *G. ferruginea* strain, isolated from a 60-m deep, unlined drinking-water well, was cultured under microaerophilic conditions to obtain biogenically formed iron oxyhydroxide precipitates. The formed bacteriogenic iron oxyhydroxides (BIOS), an intermix of *G. ferruginea* cells, stalks, extracellular exudates, and precipitated iron oxyhydroxides, was used for batch sorption experiments with uranium(VI) and neptunium(V) under anaerobic conditions. X-ray absorption spectroscopy (XAS) and ATR FT-IR were applied to identify surface complexes and their structural coordination on biogenically formed iron oxyhydroxides. The results are compared with abiotic systems to demonstrate that microaerophilic iron(II) oxidizers contribute strongly to the immobilization of radionuclides.

Materials and methods

Characterization and cultivation of *Gallionella ferruginea*

The strain of *G. ferruginea* used in this study was isolated by Lotta Hallbeck (MICANS, Sweden) from a 60-m deep, unlined drinking-water well. The well is situated in Hindås, in the southwest of Sweden. *G. ferruginea* is a stalk-forming, autotrophic, and iron-oxidizing bacterium, which was first described by Ehrenberg (1836). It is described in detail in several papers by Hallbeck and co-authors. The phylogenetic position of *Gallionellaceae* is among the β-Proteobacteria, as determined by 16S-rDNA sequence comparisons (Hallbeck et al. 1993). The cells have a curved rod shape with a size of 1.6–2.5 × 0.5–0.8 mm (Hallbeck and Pedersen 1990). The cells are Gram-negative (Teichmann 1935) with an outer membrane and a thin peptidoglycan cell wall (Hallbeck and Pedersen 2005). *G. ferruginea* can be recognized under the microscope by its twisted stalks, which are produced when iron-rich groundwater comes in contact with air at neutral pH (Hallbeck and Pedersen 2014).

The carbon source for *G. ferruginea* is carbon dioxide, and the energy and electron source is ferrous iron, which is oxidized to ferric iron with oxygen as electron acceptor. The culture of *G. ferruginea* strain, provided by MICANS, was cultivated in our laboratory. A mineral salt solution (MSS) was prepared as described by Kucera and Wolfe (1957), modified by Hanert (1981), and briefly described in Hallbeck and Pedersen (1990), consisting of 1 g NH_4Cl, 0.4 g $MgSO_4 \times 7H_2O$, 0.1 g $CaCl_2 \times 2H_2O$, 0.5 g K_2HPO_4, and 1 L Milli-Q water. The MSS medium was autoclaved and cooled to 5 °C. Several 300 mL Erlenmeyer flasks with around 150 mL MSS medium were infused with sterile-filtered CO_2 for 30 s to reach pH 4.6–4.8. After the CO_2 infusion, 600 screw-capped glass tubes (180 × 16 mm), used as culture vessels, were filled each with 10 mL MSS. Iron sulfide was prepared as described by Hanert (1981) by dissolving 7.8 g $FeSO_4(N_6H_4)_2SO_4$ (Mohr's salt) and 4.8 g Na_2S separately, each in 200 mL boiling Milli-Q water, and subsequently pouring the ferrous iron solution into the Na_2S solution. Glass Pasteur pipettes were used to add 20 drops of sterile iron sulfide solution carefully by inserting the pipette to the bottom of the tubes. When the iron sulfide had settled, the tubes were immediately inoculated with *G. ferruginea* culture. The culture was incubated at a temperature below 25 °C due to the heat sensitivity of this strain of *G. ferruginea*. The cultures were sub-cultured once a week.

Precipitation of ferric oxyhydroxide

Already within the first days of *G. ferruginea* cultivation in the tubes, a yellowish coloration was visible in the solution, indicating that ferrous iron is oxidized by the microaerophilic ferrous oxidizer *G. ferruginea* at the currently available low O_2 concentrations. As described by numerous authors (e.g., Hanert 1981; Hallbeck and Pedersen 1995; Stumm and Morgan 1996; Ferris et al. 1999; Banfield et al. 2000; Melton et al. 2014), the bacteriogenic-induced oxidation of Fe(II) leads often to a precipitation and encrustation on the twisted stalk materials of *G. ferruginea*. Iron-rich particles

with 2–3 nm diameters are formed as colloids and are attached to the negatively charged polymers of *G. ferruginea* stalks as shown by using scanning electron microscopy (SEM) in Fig. 1. Since at near-neutral pH the solubility of ferric iron compounds is low, Banfield et al. (2000) suggested that a solution supersaturation immediately could take place with respect to ferrihydrite solubility. By selected area electron diffraction (SAED), the authors were able to show that the samples mostly consisted of randomly oriented two-line ferrihydrite. During the cultivation of *G. ferruginea*, high amounts of ferric oxyhydroxide were formed as small, roundish particles (0.1–0.5 μm) within a short time in our study.

Separation of BIOS

The formed BIOS was removed from the tubes by using glass Pasteur pipettes. It was sampled in 50 mL Greiner tubes and centrifuged (Ultracentrifuge Optima XL100K, Rotor: SW 32Ti; Beckman Coulter, USA) at 187,000×*g* for 20 min. The supernatant was removed, and the BIOS was washed four times with sterile tap water. The BIOS was separated and transferred into inert gas boxes (N_2 atmosphere) for uranium and neptunium sorption experiments, respectively.

Sorption experiments with uranium(VI) and neptunium(V)

For uranium sorption experiments, 8.4 mg of the BIOS was mixed with 50 mL sterile tap water, where $UO_2(ClO_4)_2$ was added prior to achieve an initial uranium(VI) concentration of 0.09 mM. In another experiment $NpO_2(ClO_4)$ was added to 10 mL sterile tap water to reach a final neptunium(V) concentration of 0.09 mM and subsequently mixed with 5.6 mg BIOS. The pH was adjusted in each experiment to 7.8 by adding diluted NaOH solution. The suspensions were shaken on a horizontal shaker for 183 h and 185 h, respectively, at room temperature. At the beginning of the uranium(VI) sorption experiment, aliquots containing 0.5 mL of the suspension were taken every 0.5 h, since sorption of uranium(VI) on abiotic ferrihydrite is known to be very fast (Waite et al. 1994). The samples were centrifuged at 187,000×*g*, and the uranium(VI) concentration in the supernatants was determined by means of inductively coupled plasma mass spectrometry (ICP-MS) using an ELAN 9000 ICP-MS spectrometer (PerkinElmer, Überlingen, Germany) after acidification. The neptunium(V) concentration was determined by liquid scintillation counting (LSC, Winspectral α/β, Wallac 1414, Perkin Elmer, Rodgau, Germany) using α-β discrimination. For this, 100 μL of the centrifuged aliquot was taken and mixed with 5 mL Ultima Gold™ scintillation cocktail (Perkin Elmer). During the experiments, redox potentials and pH values were recorded. The pH values were measured with a conventional pH electrode (WTW SenTix 20, Germany), regularly calibrated by means of commercial buffer solutions. Redox potentials of the sample solutions were measured using a combined platinum Ag/AgCl redox electrode (WTW Electrode SenTix ORP, Germany). The data are reported as E_h values, i.e., as potentials against the standard hydrogen electrode. For reproducibility, the sorption experiments were performed in duplicate.

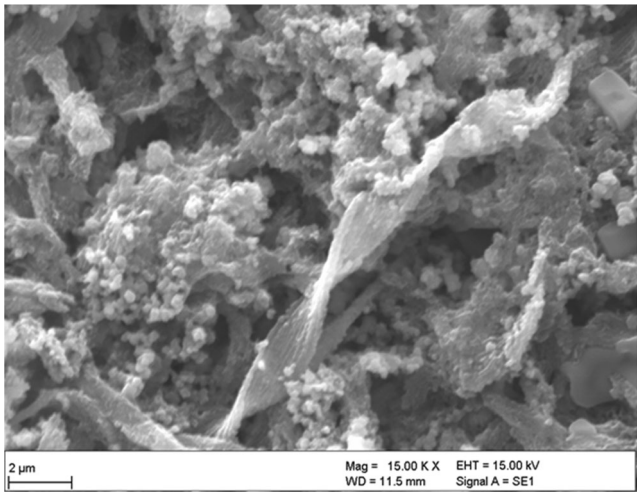

Fig. 1 SEM image of BIOS, as a mixture of G. ferruginea cells and stalks, extracellular exudates, and ferric oxyhydroxide

Thermodynamic calculation

The chemical composition of the supernatants from the uranium and neptunium sorption experiments was determined at the end of the experiments. The data were used to calculate the predominance fields of various uranium and neptunium species, respectively, at room temperature. The corresponding pH–E_h diagrams were constructed using the geochemical speciation code Geochemist's Workbench, version 12.0.4/Act2. For uranium, the database used was the thermo.dat accompanying the code, supplemented by the most recent NEA database for aqueous uranium species (Guillaumont et al. 2003) and by thermodynamic data of the aqueous species $Ca_2UO_2(CO_3)_{3(aq)}$ (Bernhard et al. 2001). This species is the major species in the area characterized by a higher pH (6.8–10.9) and a higher redox potential limit, moving from + 60 mV at pH 6.8 to − 250 mV at pH 10.9. For neptunium, thermodynamic data of the Lawrence Livermore National Laboratory thermodynamic database were supplemented by the most recent NEA database (Lemire et al. 2001; Guillaumont et al. 2003).

X-ray absorption spectroscopy

After separation of the supernatants, the U-BIOS and Np-BIOS samples were filled as wet paste into polyethylene sample holders under anoxic conditions in a glove box. The

sample holders were hot sealed and immediately shock frozen in liquid N_2. The samples were transported in a special dewar filled with liquid N_2 (Voyageur 12, Air Liquide Deutschland GmbH, Germany) to be analyzed at the Rossendorf Beamline of the European Synchrotron Radiation Facility (ESRF) in Grenoble (France) by XAS. XAS is a powerful method to provide detailed element-specific information on the speciation and local coordination environment of the probed element. It includes X-ray absorption near-edge structure (XANES) spectroscopy for detailed element-specific information on the oxidation state and site geometry through interpreting both the position and the structure of the absorption edge as well as extended X-ray absorption fine structure (EXAFS) (~ 50–1000 eV above the edge), which is used to extract detailed information on local coordination and bonding environment. It is an element-specific bulk method, giving information about the average, local structural, and compositional environment of the X-ray-absorbing atom. U L_{III}- and Np L_{III}-edge spectra of frozen pellets were collected in fluorescence mode using a 13-element germanium detector and a helium cryostat at 15 K. During fluorescence measurements, eight to ten scans were recorded for each sample and then averaged. The energy scale was calibrated using the maximum of the first derivative of the K-edge absorption spectrum of yttrium (17,038 eV). The EXAFS spectra were analyzed according to standard procedures including statistical weighting of the 13 fluorescence channels and dead-time correction using WinXAS 3.2 (Ressler 1998). In addition, the spectra were investigated with the Iterative Transformation Factor Analysis (ITFA) software package (Rossberg et al. 2003).

In situ attenuated total reflection Fourier-transform infrared spectroscopy

In situ ATR FT-IR spectroscopy with a sub-minute time resolution was performed for monitoring and complementary molecular identification of the neptunium(V) sorption process on the BIOS. Infrared spectra were measured from 1600 to 750 cm^{-1} on a Bruker Vertex 80/v vacuum spectrometer equipped with a Mercury Cadmium Telluride detector. Spectral resolution was 4 cm^{-1}, and spectra were averaged over 256 scans. A horizontal diamond crystal with nine internal reflections (DURA SamplIR II, Smiths Inc.) was used. Further details on the experimental ATR FT-IR spectroscopy setup are compiled in Müller et al. (2012). The performance of in situ sorption experiments requires a thin sample film prepared directly on the surface of the ATR diamond crystal as stationary phase. This was accomplished by pipetting 5 μL of the sample on the ATR crystal and subsequent drying with a gentle stream of N_2. Flow-through measurements at a rate of 0.1 mL min^{-1} were performed using a flow cell ($V = 200$ μL). First, the film was flushed with a blank solution (sterilized tap water, pH 8) for 60 min conditioning. In a second step, a 50 μM neptunium(V) solution (sterilized tap water, pH 5) was rinsed for sorption during the next 60 min. Finally, the neptunium(V)-loaded film was flushed again with the blank solution (60 min) in order to gain information on the reversibility of the sorbed species.

The applied principle of reaction-induced difference spectroscopy allows the detection of very small absorption changes provoked by the sorption process in comparison with the very strong absorbing background, i.e., water and sample film. Further details on the calculation of difference spectra are given in Müller et al. (2012) and Müller et al. (2013).

Results and discussion

Uranium and neptunium sorption

In our anaerobic experiments, uranium(VI) and neptunium(V) were added aseptically from an actinide stock solution to the BIOS suspension to reach an actinide concentration of 0.09 mM at a pH of 7.8. At the end of the experiments, the uranium concentration in the BIOS suspension was determined to have declined to 0.03 mM, clearly indicating that uranium had been removed from solution and immobilized on the BIOS sample. As shown in Fig. 2, most of the uranium sorption occurred during the first 24 h of the experiment, indicating a rapid initial sorption process, which is also typical for the binding of inorganic ions to abiotic ferrihydrite (Waite et al. 1994). After 183 h, a uranium uptake of 78-mg U g^{-1} dry mass was determined. An apparent bulk distribution coefficient (K_d) of 1.23×10^4 L kg^{-1} was calculated following the conventional operational definition according to Bau (1999) as the ratio between sorbed [U] per kg BIOS and dissolved [U] per L water.

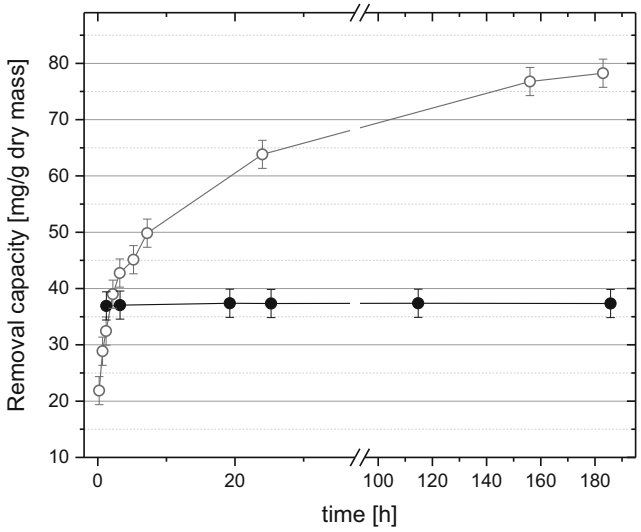

Fig. 2 Uranium (○) and neptunium (●) removal capacity of BIOS as a function of time at pH 7.8 and room temperature

For the neptunium sorption experiment, it was clearly shown that already in the first hour, neptunium was almost completely removed from the solution, which led to an uptake of 37 mg Np g^{-1} dry mass under the applied experimental conditions. The calculated apparent bulk distribution coefficient (K_d) amounts to 3.07×10^5 L kg^{-1}. The determined K_d values for uranium and neptunium result from the fact that biogenic iron oxyhydroxide samples in general consist of inorganic and organic material, where the organic material (e.g., bacteria, stalks) and their deprotonated carboxylate and phosphate functional groups provide active surface sites (Warren and Zimmerman 1994; Ferris et al. 1989). After Ferris et al. (1999), the K_d values consequently decrease with increasing iron oxyhydroxide content and decreasing content of organic material. Recent studies suggest that the higher sorption capacity of heavy metals results can be attributed to the effect of the physical and chemical characteristics of organics in BIOS (Field et al. 2019). Kikuchi et al. (2019) assume that the negatively charged BIOS are more electrostatically favorable for the adsorption of cations, such as Cs(I), than the positively charged abiogenic ferrihydrite.

Thermodynamic calculation

When plotting the measured pH and E_h values of the supernatant, which decreased from the beginning to the end of the uranium sorption experiment (pH 7.78 to 7.38 and E_h 395 ± 30 mV to 174 ± 30 mV, respectively), the predominance of an aqueous calcium uranyl carbonate species is predicted (Fig. 3), showing that uranium clearly exists in the uranium(VI) stability field. The $Ca_2UO_2(CO_3)_{3(aq)}$ species is characterized by a low sorption affinity to minerals as was shown, for instance, for ferrihydrite and quartz (Fox et al. 2006), clay (Joseph et al. 2013; Philipp et al. 2019), and granite (Schmeide et al. 2014). Brooks et al. (2003) have shown that calcium uranyl carbonate complexes inhibit microbial reduction of uranium(VI) under certain conditions. Furthermore, Singer et al. (2009, 2012) found that abiotic reduction of uranium(VI) by iron(II)-bearing minerals (magnetite and chlorite) only occurs in the absence of calcium, but it is inhibited in the presence of both, calcium and carbonate. Consequently, the presence of $Ca_2UO_2(CO_3)_3$ species in solution is the reason for the lower K_d value determined for uranium sorption onto BIOS. For the neptunium sorption experiment, the thermodynamic calculation shows that under ambient conditions, NpO_2^+ is the major species in the area characterized by a wide pH range (0–8.7) with a redox potential limit, moving from + 690 at pH 0 to 120 mV at pH 5.6 and 200 mV at pH 8.7. The pH and E_h values of the supernatant, which were measured at different times during the experiment, were plotted within the diagram (Fig. 4). The results show that already in the first hours of the experiment, the E_h value decreased from 395 ± 30 mV, which is located within the neptunium(V) stability field, towards the neptunium(V)/neptunium(IV) border with an E_h value of 174 ± 30 mV. A reduction of neptunium(V) to neptunium(IV), which would lead to an increased neptunium retention, cannot be excluded completely based on these thermodynamic data, but could be excluded by XANES (cf. paragraph 3.4. below).

In situ ATR FT-IR

The BIOS films prepared on the ATR crystal were flushed with a blank solution at the same conditions as used in the

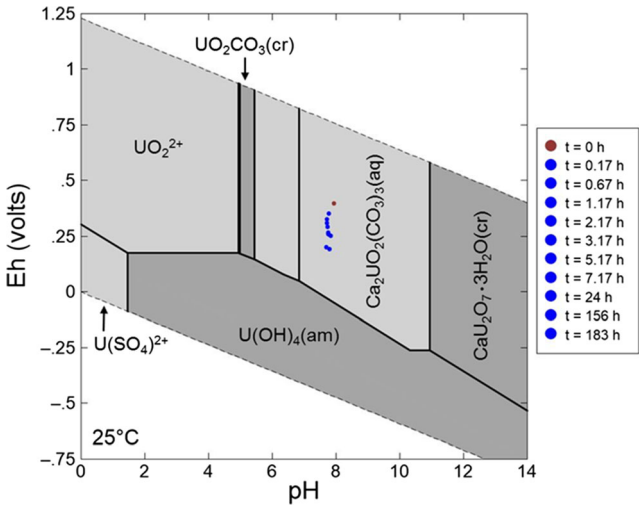

Fig. 3 pH–E_h predominance diagram for uranium species (0.09 mM uranium, at room temperature) after thermodynamic calculation using the geochemical speciation code Geochemist's Workbench Version 10.0.5/Act2 and the analytical data of the supernatant, determined at the end of the experiment. The plotted pH and E_h data correspond to the measured values in the supernatant at different times during the experiment

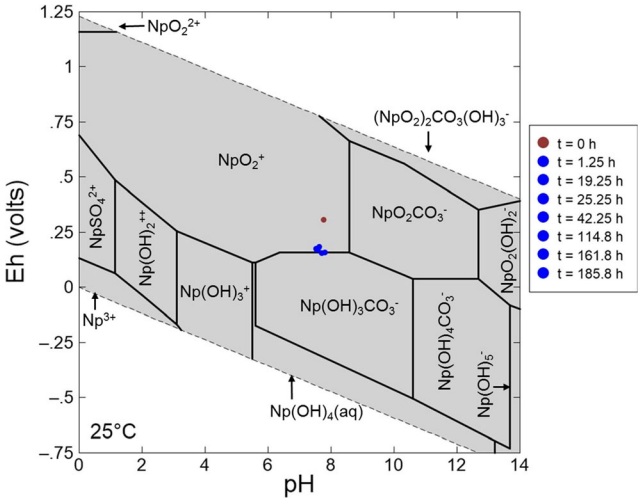

Fig. 4 pH–E_h predominance diagram for neptunium species (0.09 mM neptunium, at room temperature) after thermodynamic calculation using the geochemical speciation code Geochemist's Workbench Version 10.0.5/Act2 and the analytical data of the supernatant, determined at the end of the experiment. The plotted pH and E_h data correspond to the measured values in the supernatant at different times during the experiment

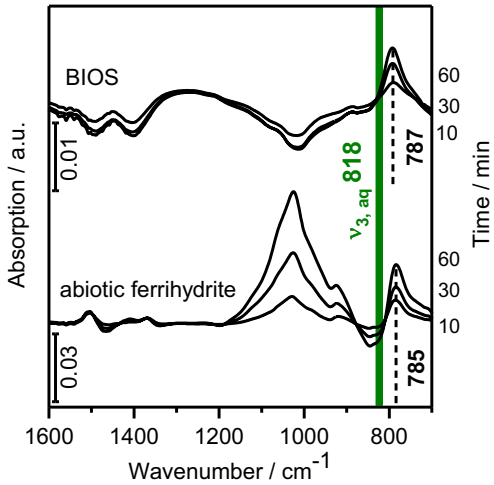

Fig. 5 In situ time-resolved mid-IR spectra of Np(V) sorption on BIOS and abiotic ferrihydrite (50 μM initial Np(V), sterilized tap water, pH 8, flow rate 0.1 mL min^{-1}). The spectra of the sorption process are recorded at various times after induction, as given. Ordinate scaling is given by the bar in units of optical density. Other values indicated are in cm^{-1}

sorption experiment. The resulting spectra after 60 min of conditioning provided no spectral features, indicating that a steady state was obtained (data not shown). The accumulation of neptunium(V) on the BIOS surface can directly be observed by the increasing band below 800 cm^{-1} upon sorption (Fig. 5). It can be assigned to the antisymmetric stretching vibrational mode ν_3 of NpO_2^+. The increasing signal and the very good signal-to-noise ratio indicate the sorption of neptunium(V). A solution species could hardly be detected at the neptunium(V) concentration of 50 μM. In aqueous solution at similar conditions, the free NpO_2^+ is present. This species shows IR absorption at 818 cm^{-1} as indicated in Fig. 5 by the green line. The shift by 31 cm^{-1} in the case of BIOS indicates a strong binding of neptunium(V) to the substrate. The same is valid for abiotic ferrihydrite as shown in Fig. 5, as well as for hematite (Müller et al. 2015). The different intensities may be due to different film heights prepared on the ATR crystal. The band arising at 1050 cm^{-1} is probably due to arrangements of surface functionalities. The reversibility of the sorption process, monitored by a flushing step with the blank solution (data not shown), showed a very small negative band at the same frequency as the band arising during sorption, i.e., at 787 cm^{-1}. This indicates that minor parts of the sorbed species are removed from the interface under the experimental conditions.

Uranium(VI) and neptunium(V) coordination environment studied with XAS

Direct structural data have been obtained with EXAFS at the uranium L_{III}-edge and the neptunium L_{III}-edge to identify the structure of uranium and neptunium species associated with the BIOS samples after the sorption experiments. In Fig. 6, the XAS spectra are shown for U-BIOS sample along with those of selected references, e.g., the bidentate edge-sharing uranyl sorption complex (^{1}E) and the aqueous uranyl tricarbonate complex ($UO_2(CO_3)_3^{4-}$). The k^3-weighted EXAFS spectrum and its Fourier-transform magnitude (Fig. 6 b and c) of the studied U-BIOS sample bears close resemblance to the bidentate edge-sharing inner-sphere sorption complex (^{1}E), which is the most prominent surface species in the absence of carbonate and the main sorption species on abiotic ferrihydrite (Rossberg et al. 2009). The tricarbonato surface complex was identified by Hiemstra et al. (2009) as a major ternary species in systems equilibrated at elevated pCO_2 and above-neutral pH, where high carbonate concentrations occur. Since CO_2 was present during the cultivation of the *G. ferruginea*

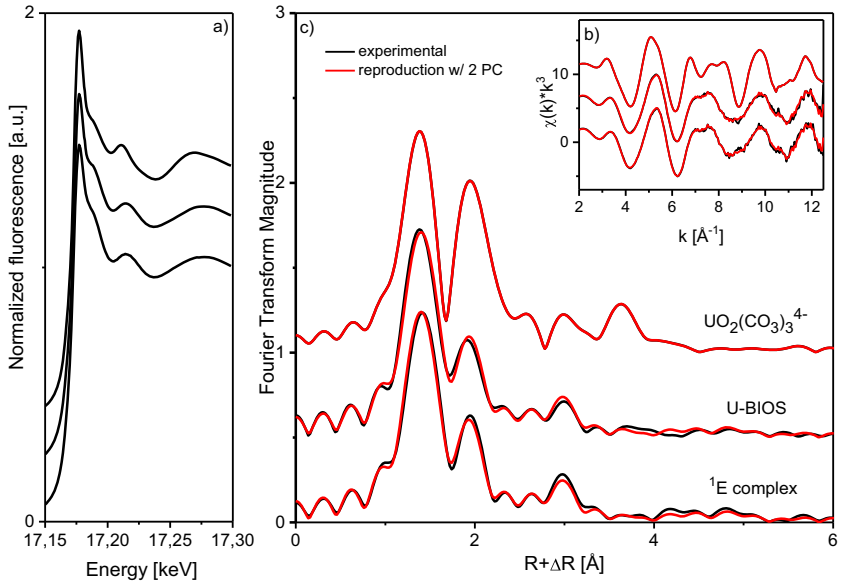

Fig. 6 Uranium L_{III}-edge XANES spectra (**a**) of the aqueous tricarbonato complex and uranyl sorption complex (^{1}E) in comparison with U-BIOS sample. Uranium L_{III} k^3-weighted EXAFS spectra (**b**) and corresponding Fourier transform (**c**) of uranium sorbed on the BIOS sample together with the endmember species observed for ferrihydrite sorption samples, i.e., a bidentate edge-sharing uranyl sorption complex (^{1}E) and the aqueous tricarbonate complex ($UO_2(CO_3)_3^{4-}$) representative for a type B ternary uranyl-carbonato sorption complex taken from Rossberg et al. (2009)

Table 1 Uranium L_{III} and Neptunium L_{III} EXAFS shell fit results of BIOS samples (S_0^2 = 0.9, fit range 2.0–12.5 $Å^{-1}$)

Sample	O shell			Fe shell			ΔE_0 [eV][d]	χ^2 res [%] [e]
	CN[a]	R [Å][b]	σ^2 [$Å^2$][c]	CN	R [Å][b]	σ^2 [$Å^2$][c]		
U-BIOS	2.0[f] O	1.79	0.0017	0.5	3.44	0.0080	11.9	14.6
	5.0 O	2.34	0.0100					
Np-BIOS	2.0[f] O	1.86	0.0016	1.5	3.39	0.0100	13.6	13.5
	5.2 O	2.44	0.0094					

[a] CN: coordination number, error ± 25%

[b] R: radial distance, error ± 0.01 Å

[c] σ^2 : Debye-Waller factor, error ± 0.0005 $Å^2$

[d] ΔE_0: shift in threshold energy

[e] χ^2 res: normalized least squares residual

[f] Parameters were fixed in the data fitting

strain, the BIOS formed in this system may have a relatively high carbonate loading on its surface. This carbonate loading might cause the formation of a small portion of the uranyl-carbonato sorption complex. To elucidate the presence of a second sorption species, we performed iterative transformation factor analysis (ITFA) using the spectra of the ^{1}E uranyl ferrihydrite sorption complex and the uranyl-carbonato sorption complex as endmember species. The good reproduction of the U-BIOS spectrum by applying only two principal components (compare the black and red lines in Fig. 6 b and c) is a proof that only two species are present and that these are represented by the two endmember species. Furthermore, we determined by using ITFA that the ^{1}E complex is in fact predominant with 95%, while only 5% of the ternary uranyl-carbonato complex is present. Correspondingly, the shell fit showed only the local structure of the ^{1}E complex. The XANES position and especially its fine structure as shown in Fig. 6(a) are indicative of the hexavalent uranyl moiety, as it was expected according to the thermodynamic calculation of the uranium-BIOS suspension. Hence, the spectrum shows no indication for a significant amount of uranium(IV) in the U-BIOS sample. The EXAFS structural parameters (see Table 1) obtained from the theoretical curve fit indicate the formation of a bidentate inner-sphere complex. The fit of the first and second oxygen shell of the uranium L_{III}-edge EXAFS spectrum showed five equatorial (eq) oxygen atoms with an average U–O_{eq} distance of 2.34 Å and two axial (ax) oxygen atoms at a U–O_{ax} distance of 1.79 Å. The appearance of O_{ax} and O_{eq} verifies the hexavalent oxidation state of uranium. The short radial U–Fe distance of 3.44 Å indicates a bidentate edge-sharing linkage of the UO_2^{2+} cation to an $Fe(O,OH)_6$ octahedron (Fig. 7).

In our study, the neptunium(V) species on the BIOS surface have also been identified as mononuclear, inner-sphere complexes (see Fig. 8 b and c), since no Np–Np interaction but a Np–Fe interaction at 3.39 Å could be detected. The structural parameters based on the shell fit analysis (Table 1) showed an average of five oxygen atoms at a Np–O_{eq} distance of 2.44 Å, two oxygen atoms at a Np–O_{ax} distance of 1.86 Å, and iron atoms at a Np–Fe distance of 3.39 Å. The Np–Fe distance is also in accord with a bidentate edge-sharing inner-sphere surface complex of the NpO_2^+ cation to an $Fe(O,OH)_6$ octahedron (Fig. 7). Also, the XANES spectrum of the sample, which was treated with neptunium (Fig. 8a), does not show any indication for significant amount of Np(IV). The "yl-shoulder" is fully expressed at about 17,630 keV.

Comparison of abiotic iron oxides and oxyhydroxides with BIOS samples

The radial U–O_{ax} and U–O_{eq} distances of the studied U-BIOS sample were compared with those of abiotic or synthesized

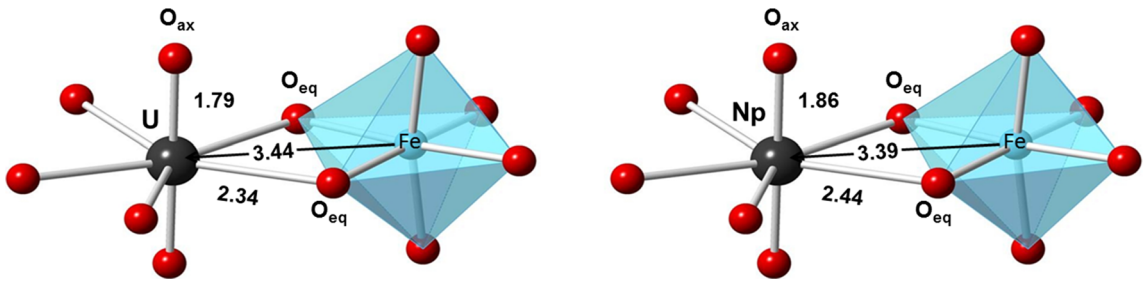

Fig. 7 Structural models of the sorption complexes with radial distances for U-BIOS and Np-BIOS, where the UO_2^{2+} ion or the NpO_2^+ ion bound via edge-sharing to one $Fe(O,OH)_6$ octahedron

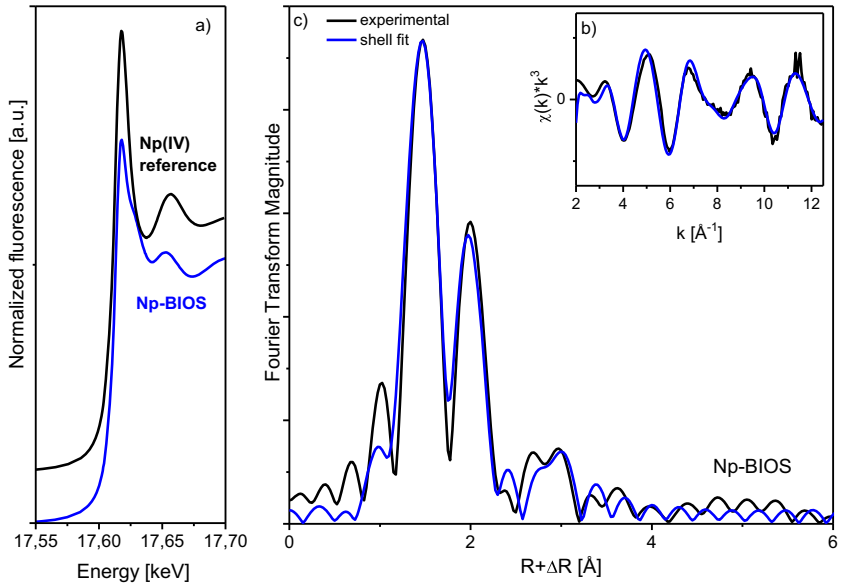

Fig. 8 Neptunium L_{III}-edge k^3-weighted EXAFS spectrum (b, black) and corresponding Fourier transform (c) of neptunium sorbed on the BIOS sample; shell fits (blue). Neptunium L_{III}-edge XANES spectrum (a) of Np-BIOS sample in comparison with a neptunium(IV) reference

iron oxides and iron oxyhydroxides determined at neutral pH. As shown in Table 2, the distances determined for U-BIOS are similar to those of abiotic ferrihydrite samples determined by Waite et al. (1994) and Rossberg et al. (2009), considering that the errors in determination of EXAFS interatomic distances and coordination numbers have an uncertainty of 0.01−0.02 Å and 10–35%, respectively. Similar distances were also measured for abiotic ferrihydrite by Ulrich et al. (2006). Recent EXAFS studies of uranium sorption on ferrihydrite by Winstanley et al. (2018) can also be used for comparison, noting however that the studies were performed under alkaline conditions and using uranium concentrations up to 1.05 mM, where precipitation of a discrete U(VI) phase was detected. However, the sorption mechanism was also described as uranium sorption to ferrihydrite via a bidentate edge-sharing inner-sphere species with carbonate forming a ternary surface complex. A splitting of the O_{eq} shell as shown for abiotic goethite, lepidocrocite, maghemite, and magnetite could only be detected in abiotic ferrihydrite samples by Waite et al. (1994). Neither the samples examined by Rossberg et al. (2009) nor the BIOS sample permits the detection of a splitting of the equatorial oxygen shell. Compared with the results reported for uranium(VI), only few EXAFS studies on the adsorption of neptunium(V) on iron oxides have been conducted at circumneutral pH, whereas no EXAFS studies have been conducted on the sorption of neptunium(V) on ferrihydrite in the near-neutral pH range. In the BIOS sample, the fitting of the first and second oxygen shell of the neptunium L_{III}-edge EXAFS spectrum showed five oxygen atoms with an average Np–O_{eq} distance of 2.44 Å and two oxygen atoms at a Np–O_{ax} distance of 1.86 Å (see Table 3). The O_{ax} bond lengths are shorter than those observed for Np(V) adsorbed to hematite (Müller et al. 2015; Amayri et al. 2007) and goethite (Combes et al. 1992). According to Bots et al. (2016), this

Table 2 Distances of the coordination shells of U-containing BIOS in comparison with abiotic iron oxides and iron oxyhydroxides

	Ferrihydrite [1]	Ferrihydrite [2]	Ferrihydrite [3]	Abiotic Goethite [4]	Lepidocrocite [4]	Maghemite [4]	Magnetite [4]	Biogenic BIOS [5]
U–O_{ax}	1.80 Å	1.80 Å	1.82 Å	1.82 Å	1.77 Å	1.83 Å	1.78 Å	1.79 Å
U–O_{eq1}	2.35 Å	2.35 Å	2.38 Å	2.26 Å	2.31 Å	2.28 Å	2.26 Å	2.34 Å
U–O_{eq2}				2.51 Å	2.54 Å	2.55 Å	2.52 Å	–
U–Fe	3.41 Å	3.41 Å	3.46 Å		3.44 Å			3.44 Å

[1] Waite et al. (1994)
[2] Rossberg et al. (2009);
[3] Winstanley et al. (2018)
[4] Dodge et al. (2002)
[5] This study
Radial distance error ± 0.01 Å

Table 3 Distances of the coordination shells of Np-containing BIOS in comparison with abiotic iron oxides and iron oxyhydroxides at circumneutral pH and for ferrihydrite at pH 9.5 and 11

	Abiotic			Biogenic		
	Lepidocrocite [1]	Hematite[2][a]	Hematite [3][a,b]	Goethite [4]	Ferrihydrite [5]	BIOS [6]
Np–O_{ax}	1.80–1.85	1.88 Å	1.87 Å	1.85	1.83–1.85	1.86 Å
Np–O_{eq1}	2.44–2.46	2.47 Å[c]/2.46 Å[d]	2.48 Å	2.51	2.38–2.42	2.44 Å
Np–O_{eq2}		2.46 Å	2.84 Å	–		–
Np–Fe	3.45	3.47 Å[c]/3.73 Å[d]	3.44 Å[b]/3.73 Å[a]			3.39 Å

[a] Inert

[B] air

[c] Fit model 1

[d] Fit model 2, radial distance error ± 0.01 Å

[1] Yang et al. (2015)

[2] Müller et al. (2015)

[3] Amayri et al. (2007)

[4] Combes et al. (1992)

[5] Bots et al. (2016)

[6] This study

could be caused by positively charged neptunyl, forming stronger and consequently shorter bonds with negatively charged hydroxide than with the oxygen of water molecules. EXAFS studies on neptunium(V)-ferrihydrite were exclusively carried out under alkaline conditions (pH 9.5 and 11) by Bots et al. (2016). The Np–O axial bond length and the Np–O equatorial oxygen distance of the alkaline ferrihydrite samples ranged from 1.83 to 1.85 Å and 2.38 to 2.42 Å, respectively. This is in accordance with the distances we have received by fitting the EXAFS data of the BIOS sample, hence neptunium(V) sorbs in the BIOS sample also via an inner-sphere bidentate mononuclear surface complex at the ferrihydrite surface.

Conclusions

BIOS samples, which were formed by a *G. ferruginea* strain at circumneutral pH values, were used for uranium(VI) and neptunium(V) sorption experiments. The XAS analyses showed that both uranium(VI) and neptunium(V) were sorbed by forming a bidentate edge-sharing inner-sphere sorption complex on ferrihydrite. A small fraction (5%) of uranyl also sorbed to ferrihydrite as the previously observed uranyl-carbonato complex. No influence of the organic components of BIOS on the surface speciation was found by XAS. The existence of *G. ferruginea* is of great importance for the formation of larger amounts of ferrihydrite compared with abiotic systems, resulting in numerous adsorption surface sites. The results presented here contribute to a better understanding of the potential role of BIOS in natural environments. The radionuclide adsorption observed for BIOS samples is relevant to various environmental conditions. Thus, BIOS can be regarded as an environmental barrier to prevent migration of actinides in general in radioactively contaminated sites or in the far-field of nuclear waste repositories and consequently, should be considered in developing remediation strategies and performing risk assessments.

Acknowledgments We thank Sabrina Beutner and Carola Eckardt for ICP-MS analyses and DIC measurements and Karsten Heim (all from HZDR) for in situ ATR FT-IR measurements.

Funding information Open Access funding enabled and organized by Projekt DEAL. The research leading to these results has received funding from the European Union's European Atomic Energy Community's (Euratom) Seventh Framework Programme FP7/2007-2011 under grant agreement no. 269658 (CROCK project).

Open Access This article is licensed under a Creative Commons Attribution 4.0 International License, which permits use, sharing, adaptation, distribution and reproduction in any medium or format, as long as you give appropriate credit to the original author(s) and the source, provide a link to the Creative Commons licence, and indicate if changes were made. The images or other third party material in this article are included in the article's Creative Commons licence, unless indicated otherwise in a credit line to the material. If material is not included in the article's Creative Commons licence and your intended use is not permitted by statutory regulation or exceeds the permitted use, you will need to obtain permission directly from the copyright holder. To view a copy of this licence, visit http://creativecommons.org/licenses/by/4.0/.

References

Amayri S, Breckheimer M, Drebert J, Reich T (2007) EXAFS study of Np(V) sorption onto hematite (α-Fe_2O_3). Wissenschaftliche Berichte FZKA 7360, Annual Report 2006:163

Anderson CR, Pedersen K (2003) In situ growth of *Gallionella* biofilms and partitioning of lanthanides and actinides between biological material and ferric oxyhydroxides. Geobiology 1:169–178

Anderson CR, James RE, Fru EC, Kennedy CB, Pedersen K (2006) In situ ecological development of a bacteriogenic iron oxide-producing microbial community from a subsurface granitic rock environment. Geobiology 4:29–42

Ankrah DA, Søgaard EG (2009) A review of biological iron removal. Thirteenth International Water Technology Conference, IWTC 13 2009, Hurghada, Egypt

Banfield JF, Welch SA, Zhang H, Ebert TT, Penn RL (2000) Aggregation-based crystal growth and microstructure development in natural iron oxyhydroxide biomineralization products. Science 289:751–754

Bau M (1999) Scavenging of dissolved yttrium and rare earth elements by precipitating iron oxyhydroxide: experimental evidence for Ce oxidation, Y-Ho fractionation, and lanthanide tetrad effect. Geochim Cosmochim Acta 63:66–77

Bernhard G, Geipel G, Reich T, Brendler V, Amayri S, Nitsche H (2001) Uranyl(VI) carbonate complex formation: validation of the $Ca_2UO_2(CO_3)_{3(aq.)}$ species. Radiochim Acta 89:511–518

Bots P, Shaw S, Law GTW, Marshall TA, Mosselmans JFW, Morris K (2016) Controls on the fate and speciation of Np(V) during iron (oxyhydr)oxide crystallization. Environ Sci Technol 2016(50): 3382–3390

Brooks SC, Fredrickson JK, Carroll SL, Kennedy DW, Zachara JM, Plymale AE, Kelly SD, Kemner KM, Fendorf S (2003) Inhibition of bacterial U(VI) reduction by calcium. Environ Sci Technol 37: 1850–1858

Chan CS, De Stasio G, Welch SA, Girasole M, Frazer BH, Nesterova MV, Fakra S, Banfield JF (2004) Microbial polysaccharides template assembly of nanocrystal fibers. Science 303:1656–1658

Chan CS, Fakra SC, Emerson D, Fleming EJ, Edwards KJ (2011) Lithotrophic iron-oxidizing bacteria produce organic stalks to control mineral growth: implications for biosignature formation. ISME J 5:717–727

Combes J-M, Chisholm-Brause CJ, Brown GE, Parks GA, Conradson SD, Eller PG, Trlay IR, Hobart DE, Meljer A (1992) EXAFS spectroscopic study of neptunium(V) sorption at the a-FeOOH/water interface. Environ Sci Technol 26:376–382

Dodge CJ, Francis AJ, Gillow JB, Halada GP, Eng C, Clayton CR (2002) Association of uranium with iron oxides typically formed on corroding steel surfaces. Environ Sci 36(16):3504–3511

Edwards KJ, Rogers DR, Wirsen CO, McCollom TM (2003) Isolation and characterization of novel psychrophilic, neutrophilic, fe-oxidizing, chemolithoautotrophic α- and γ-*Proteobacteria* from the deep sea. Appl Environ Microbiol 69(5):2906–2913

Eggerichs T, Opel O, Otte T, Ruck W (2014) Interdependencies between biotic and abiotic ferrous iron oxidation and influence of pH, oxygen and ferric iron deposits. Geomicrobiol J 31:461–472

Ehrenberg G (1836) Vorlaufige Mitteilung iiber das wirkliche Vorkommen fossiler Infusorien und ihre grosse Verbreitung. Ann Phys 38(2):13–227

Emerson D, Moyer C (1997) Isolation and characterization of novel iron-oxidizing bacteria that grow at circumneutral pH. Appl Environ Microbiol 63(12):4784–4792

Ferris FG, Schultze S, Witten TC, Fyfe WS, Beveridge TJ (1989) Metal interactions with microbial biofilms in acidic and neutral pH environments. Appl Environ Microbiol 55(5):1249–1257

Ferris FG, Konhauser KO, Lyvén B, Pedersen K (1999) Accumulation of metals by bacteriogenic iron oxides in a subterranean environment. Geomicrobiol J 16:181–192

Ferris FG, Hallberg RO, Lyvén B, Pedersen K (2000) Retention of strontium, cesium, lead and uranium by bacterial iron oxides from a subterranean environment. Appl Geochem 15:1035–1042

Field HR, Whitaker AH, Henson JA, Duckworth OW (2019) Sorption of copper and phosphate to diverse biogenic iron (oxyhydr) oxide deposits. Sci Total Environ 697:134111

Fleming EJ, Langdon AE, Martinez-Garcia M, Stepanauskas R, Poulton NJ, Masland EDP, Emerson D (2011) What's new is old: resolving the identity of *Leptothrix ochracea* using single cell genomics, pyrosequencing and FISH. PLoS ONE 6(3):e17769

Fox PM, Davis JA, Zachara JM (2006) The effect of calcium on aqueous uranium(VI) speciation and adsorption to ferrihydrite and quartz. Geochim Cosmochim Acta 70:1379–1387

Girvin DC, Ames LL, Schwab AP, McGarrah JE (1991) Neptunium adsorption on synthetic amorphous iron oxyhydroxide. J Colloid Interface Sci 141(1):67–78

Guillaumont R, Fanghänel T, Fuger J, Grenthe I, Neck V, Palmer DA, Rand MH (2003) Update on the chemical thermodynamics of uranium, neptunium, plutonium, americium and technetium. In: Chemical Thermodynamics, vol. 5 (ed. OECD Nuclear Energy Agency). Elsevier, Amsterdam

Hallbeck L, Pedersen K (1990) Culture parameters regulating stalk formation and growth rate of *Gallionella ferruginea*. J Gen Microbiol 136:1675–1680

Hallbeck L, Pedersen K (1995) Benefits associated with the stalk of *Gallionella ferruginea*, evaluated by comparison of a stalk-forming and a non-stalk-forming strain and biofilm studies in situ. Microb Ecol 30:257–268

Hallbeck L, Pedersen K (2005) Genus I. *Gallionella* Ehrenberg 1838 166[AL]. In: Brenner DJ, Krieg NR, Staley JT (eds) Bergey's manual of systematic bacteriology. Volume two: the proteobacteria. Part C: the alpha-, beta-, delta- and epsilonproteobacteria. Springer, New York, pp 880–886

Hallbeck L, Pedersen K (2014) The Family *Gallionellaceae*. In: Rosenberg E, DeLong EF, Lory S, Stackebrandt E, Thompson F (eds) The Prokaryotes. Springer, Berlin Heidelberg, pp 853–858

Hallbeck L, Stahl F, Pedersen K (1993) Phylogeny and phenotypic characterization of the stalk-forming and iron-oxidizing bacterium *Gallionella ferruginea*. J Gen Microbiol 139:1531–1535

Hanert HH (1981) The Genus *Gallionella*. In: Starr MP, Stolp H, Trüper HG, Balows A, Schlegel HG (eds) The Prokaryotes. Springer, Berlin, Heidelberg, pp 509–515

Hanert HH (1992) The Genus *Gallionella*. In: Balows A, Trüper HG, Dworkin M, Harder W, Schleifer KH (eds) The Prokaryotes. Springer, New York, pp 4082–4088

Hiemstra T, Van Riemsdijk WH, Rossberg A, Ulrich KU (2009) A surface structural model of ferrihydrite II: adsorption of uranyl and carbonate. Geochim Cosmochim Acta 73(15):4423–4436

Joseph C, Stockmann M, Schmeide K, Sachs S, Brendler V, Bernhard G (2013) Sorption of U(VI) onto Opalinus Clay: effects of pH and humic acid. Appl Geochem 36:104–117

Kaszuba JP, Runde WH (1999) The aqueous geochemistry of neptunium: dynamic control of soluble concentrations with applications to nuclear waste disposal. Environ Sci Technol 33:4427–4433

Kikuchi S, Kashiwabara T, Shibuya T, Takahashi Y (2019) Molecular-scale insights into differences in the adsorption of cesium and selenium on biogenic and abiogenic ferrihydrite. Geochim Cosmochim Acta 251:1–14

Kucera S, Wolfe R (1957) A selective enrichment method for *Gallionella ferruginea*. J Bacteriol 74(3):344–349

Lemire RJ, Fuger J, Nitsche H, Potter P, Rand MH, Rydberg J, Spahiu K, Sullivan JC, Ullmann WJ, Vitorge P, Wanner H (2001) Chemical thermodynamics of neptunium and plutonium. Elsevier, Amsterdam

Lieser KH, Mühlenweg U (1988) Neptunium in the hydrosphere and in the geospher. I. Chemistry of neptunium in the hydrosphere and sorption of neptunium from groundwaters on sediments under aerobic and anaerobic conditions. Radiochim Acta 43:27–35

Lloyd JR, Yong P, Macaskie LE (2000) Biological reduction and removal of Np(V) by two microorganisms. Environ Sci Technol 34:1297–1301

Marshall TA, Morris K, Law GTW, Livens FR, Mosselmans JFW, Bots P, Shaw S (2014) Incorporation of uranium into hematite during crystallization from ferrihydrite. Environ Sci Technol 48:3724–3731

Melton ED, Swanner ED, Behrens S, Schmidt C, Kappler A (2014) The interplay of microbially mediated and abiotic reactions in the biogeochemical Fe cycle. Nat Rev Microbiol 12:797–808

Müller K, Foerstendorf H, Meusel T, Brendler V, Lefèvre G, Comarmond MJ, Payne TE (2012) Sorption of U(VI) at the TiO_2–water interface: an in-situ vibrational spectroscopic study. Geochim Cosmochim Acta 76:191–205

Müller K, Foerstendorf H, Brendler V, Rossberg A, Stolze K, Gröschel A (2013) The surface reactions of U(VI) on gamma-Al_2O_3–in-situ spectroscopic evaluation of the transition from sorption complexation to surface precipitation. Chem Geol 357:75–84

Müller K, Gröschel A, Rossberg A, Bok F, Franzen C, Brendler V, Foerstendorf H (2015) In situ spectroscopic identification of neptunium(V) inner-sphere complexes on the hematite-water interface. Environ Sci Technol 49:2560–2567

Nelson YM, Lo W, Lion LW, Shuler ML, Ghiorse WC (1995) Lead distribution in a simulated aquatic environment: effects of bacterial biofilms and iron oxide. Water Res 29(8):1934–1944

Pedersen K (1997) Microbial life in deep granitic rock. FEMS Microbiol Rev 20:399–414

Pedersen K, Karlsson F (1995) Investigations of subterranean microrganisms. Stockholm, Sweden: Swedish Nuclear Fuel and Waste Management Company (SKB). Report no. 95–10:pp 222

Philipp T, Shams Aldin Azzam S, Rossberg A, Huittinen N, Schmeide K, Stumpf T (2019) U(VI) sorption on Ca-bentonite at (hyper)alkaline conditions–spectroscopic investigations of retention mechanisms. Sci Total Environ 676:469–481

Ressler T (1998) WinXAS: a program for X-ray absorption spectroscopy data analysis under MS-Windows. J Synchrotron Radiat 5:118–122

Rossberg A, Reich T, Bernhard G (2003) Complexation of uranium(VI) with protocatechuic acid-application of iterative transformation factor analysis to EXAFS spectroscopy. Anal Bioanal Chem 376:631–638

Rossberg A, Ullrich K-U, Weiss S, Tsushima S, Hiemstra T, Scheinost A (2009) Identification of uranyl surface complexes on ferrihydrite: advanced EXAFS data analysis and CD-MUSIC modeling. Environ Sci Technol 43:1400–1406

Schmeide K, Gürtler S, Müller K, Steudtner R, Joseph C, Bok F, Brendler V (2014) Interaction of U(VI) with Äspö diorite: a batch and *in situ* ATR FT-IR sorption study. Appl Geochem 49:116–125

Singer DM, Maher K, Brown GE Jr (2009) Uranyl chlorite sorption/desorption: evaluation of different U(VI) sequestration processes. Geochim Cosmochim Acta 73:5989–6007

Singer E, Emerson D, Webb EA, Barco RA, Kuenen JG, Nelson WC, Chan CS, Comolli LR, Ferriera S, Johnson J, Heidelberg JF, Edwards KJ (2011) *Mariprofundus ferrooxydans* PV-1 the first genome of a marine Fe(II) oxidizing zetaproteobacterium. PLoS ONE 6(9):e25386

Singer DM, Chatman SM, Ilton ES, Rosso KM, Banfield JF, Waychunas GA (2012) U(VI) sorption and reduction kinetics on the magnetite (111) surface. Environ Sci Technol 46:3821–3830

Søgaard EG, Medenwaldt R, Abraham-Peskir JV (2000) Conditions and rates of biotic and abiotic iron precipitation in selected Danish freshwater plants and microscopic analysis of precipitate morphology. Water Res 34:2675–2682

Sowers TD, Harrington JM, Polizzotto ML, Duckworth OW (2017) Sorption of arsenic to biogenic iron (oxyhydr)oxides produced in circumneutral environments. Geochim Cosmochim Acta 198:194–207

Stumm W, Morgan JJ (1996) Aquatic chemistry, chemical equilibria and rates in natural waters, 3rd edn. Wiley, New York

Teichmann E (1935) Vergleichende Untersuchungen über die Kultur und Morphologie einiger Eisenorganismen. Dissertation, Universität Prague

Ulrich K-U, Rossberg A, Foerstendorf H, Zänker H, Scheinost AC (2006) Molecular characterization of uranium(VI) sorption complexes on iron(III)-rich acid mine water colloids. Geochim Cosmochim Acta 70:5469–5487

Waite TD, Davis JA, Payne TE, Waychunas GA, Xu N (1994) Uranium(VI) adsorption to ferrihydrite: application of a surface complexation model. Geochim Cosmochim Acta 58:5465–5478

Warren LA, Zimmerman AP (1994) The importance of surface area in metal sorption by oxides and organic matter in a heterogeneous natural sediment. Appl Geochem 9:245–254

Weiss JV, Rentz JA, Plaia T, Neubauer SC, Merrill-Floyd M, Lilburn T, Bradburne C, Megonigal JP, Emerson D (2007) Characterization of neutrophilic Fe(II)-oxidizing bacteria isolated from the rhizosphere of wetland plants and description of *Ferritrophicum radicicola* gen. nov. sp. nov., and *Sideroxydans paludicola* sp. nov. Geomicrobiol J 24:559–570

Whitaker AH, Peña J, Amorb M, Duckworth OW (2018) Cr(VI) uptake and reduction by biogenic iron (oxyhydr)oxides. Environ Sci Process Impacts 20:1056

Winstanley EH, Morris K, Mill LGA, Blackham R, Shaw S (2018) U(VI) sorption during ferrihydrite formation: underpinning radioactive effluent treatment. J Hazard Mater 366:98–104

Yang C, Powell BA, Zhang S, Rao L (2015) Surface complexation modelling of neptunium(V) sorption to lepidocrocite (-FeOOH). Radiochim Acta 103(10):707–717

Publisher's note Springer Nature remains neutral with regard to jurisdictional claims in published maps and institutional affiliations.